A New Approach to Sign-Bit Based Parameter Estimation in OFDM Receivers

Diaz, Isael; Wilhelmsson, Leif; Sofotasios, Paschalis; Miao, Yun; Tan, Siyu; Edfors, Ove; Öwall, Viktor

Published in:
Circuits, Systems, and Signal Processing

DOI:
10.1007/s00034-015-0025-5

2015

Noname manuscript No.
(will be inserted by the editor)

A new approach to Sign−Bit based parameter estimation in OFDM receivers

Isael Diaz · Leif R. Wilhelmsson · Paschalis C. Sofotasios · Yun Miao · Siyu Tan · Ove Edfors · Viktor Öwall

Received: date / Accepted: date

Abstract This article combines algorithm development, thorough analysis and implementation of Sign-Bit (SB) estimation techniques for symbol timing, Carrier Frequency Offset (CFO) and Signal-to-Noise Ratio (SNR) in Orthogonal Frequency Division Multiplexing (OFDM) receivers. The SB estimation is compared in terms of performance and hardware complexity to an equivalent implementation with higher quantization. The techniques are demonstrated by simulation of a SB time/frequency and SB-SNR estimator for 3rd Generation Partnership Project (3GPP) Long Term Evolution (LTE) cell search in 65 nm technology operating at nominal voltage of 1.2 volts. According to post-layout power simulations with toggling information, the architecture estimates the corresponding CFO, and SNR for as little as 479 μW average power for LTE-R8/10, while occupying a silicon area as small as 0.03 mm^2. Even though SB-estimation experiences some relative performance penalty when compared to 8-Bit quantization, this paper demonstrates various advantages and the potential of employing these techniques in low complexity terminals.

Keywords OFDM · CFO · Symbol Timing · Receiver Design · Time Synchronization · SNR · LTE

I. Diaz, Y. Miao, S. Tan, O. Edfors and V. Öwall
Department of Electrical and Information Technology,
Lund University, Sweden
E-mail: {isael.diaz; ove.edfors; viktor.owall}@eit.lth.se,
E-mail: {siyu.tan.808; yun.miao.487}@student.lu.se

L. R. Wilhelmsson
Ericsson Research,
Scheelevägen 19,
SE-221 83 Lund, Sweden
E-mail: leif.r.wilhelmsson@ericsson.com

P. C. Sofotasios
Department of Electronics and Communications Engineering,
Tampere University of Technology,
FI-33101 Tampere, Finland
E-mail: paschalis.sofotasios@tut.fi

1 Introduction

Mobile terminals are in general subject to demanding constraints related to area, power and throughput. Although architectures and algorithms typically employ fixed-point arithmetic to address those stringent requirements, determining the optimum word-length that yields maximum performance at minimum cost is remarkably cumbersome since it constitutes a non-deterministic polynomial-time hard (NP-Hard) problem [9]. The procedure of selecting the best word-length typically involves the definition of an error boundary (maximum acceptable error), a cost function, and estimation of which word-length meets requirements within the error boundary either, heuristically [10], or analytically [34][33].

OFDM is an emerging technology that is regarded as the standard technique for high data-rates and high-mobility applications, particularly in hand-held devices driven by batteries. This has led to an increased industrial and academic interest towards finding effective and robust methods for improving the energy consumption in OFDM receivers. Motivated by the above, the present work is based on a purely new approach in the word-length selection process, which embraces extreme quantization and acts upon the error boundaries by systematic manipulation of the estimation algorithm. As a result, the corresponding performance degradation is controlled and traded-off with minimum area and reduced power dissipation. It is noted here that the proposed algorithms are not a straight-forward implementation of the more traditional higher precision counter-parts. Indeed, the proposed SB estimation techniques are modified accordingly in order to assure its appropriate functionality under realistic scenarios. These modification are novel and are backed-up with a corresponding mathematical analysis which is validated through comparisons with results from computer simulations.

More specifically, SB estimation is analyzed in the context of low-complexity OFDM receivers where its potential is demonstrated by performance comparison and post-layout functional simulations. To this end, three critical parameters in establishing efficient and reliable communication, namely, symbol-timing, CFO, and SNR are estimated with the aid of SB only. Note that in a real terminal a larger set of parameters or non-idealities are present, which are described and modelled in detail in [15]. However, SB estimation and its potential can be easily demonstrated for symbol-timing, CFO, and SNR.

It is recalled here that CFO and SNR estimators can be classified based on the type of data used for estimation (data-aided or blind), and the domain where the estimation takes place (time or frequency). The main drawback of frequency-domain estimators is higher complexity when compared to those operating in time-domain. This is evident in [3] and [17], where a cost function based on frequency-domain interference is used for CFO estimation. On the contrary, time-domain estimators are typically simpler and they can estimate symbol timing in addition to CFO such as in [22], [19] and [5]. Considering the above, the methods presented in this work belong to the classification of time-domain blind estimators as time-domain guarantees low complexity and blind provides a generality to the estimation covering all existing OFDM standards.

The remainder of the paper is organized as follows: The basic properties and characteristics of OFDM are revisited in Section 2. Then, the article can be considered of consisting of two main parts, even though they are not explicitly specified. The first describes the implementation of algorithm and hardware, in sections 3 and 4, respectively. The second part contains discussion and analysis of performance and complexity trade-offs in sections 5 and 6, respectively. Finally, conclusions are provided in Section 7.

2 OFDM System

Parts of a typical receiver are depicted in Fig. 1 where in each front-end the signal from one antenna is amplified, filtered, down-converted and digitized. Subsequently, symbol timing and CFO are estimated and compensated with the initial process being typically referred to as time-frequency synchronization during acquisition [24]. Efficient and robust synchronization is typically assisted by the use of pilot symbols/tones or a preamble. This has led to the design of numerous techniques based on pilots, see [26] [19] [8] [14] and more recently the work presented in [20]. However, the present work refers to a wider range of emerging communication systems that employ a Cyclic Prefix (CP), which has been adopted by all OFDM standards.

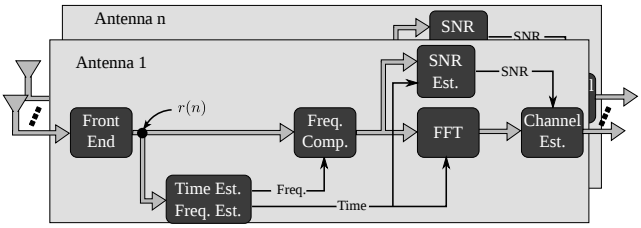

Fig. 1: A generic OFDM system.

The modulation function of an OFDM system, containing a total of T samples per symbol, is defined as,

$$g_k(n) = \begin{cases} \frac{1}{\sqrt{N}} e^{j2\pi kn/N} & \text{if } n \in [0,T) \\ 0 & \text{otherwise} \end{cases}, \tag{1}$$

where $T = N + L$, with N as the total number of subcarriers and L the length of the CP, note that $g_k(n) = g_k(n+N)$, when $n \in [0,L)$, i.e., inside the CP. Then, it follows that the complex baseband signal of the lth OFDM symbol is represented as,

$$s_l(n) = \sum_{k=0}^{N-1} x_{k,l} g_k(n - lT), \tag{2}$$

where $x_{k,l}$ denotes the modulated data subcarrier k of the lth symbol. The representation of the baseband signal with infinite duration, and thus, with infinite number of OFDM symbols is described as,

$$s(n) = \sum_{l=-\infty}^{\infty} s_l(t) = \sum_{l=-\infty}^{\infty} \sum_{k=0}^{N-1} x_{k,l} g_k(n - lT) \tag{3}$$

The corresponding received signal in time-domain, directly after the front-end as shown in Fig. 1, can be expressed as follows,

$$r(n) = h(n-\tau) * s(n) e^{j2\pi\Delta\varphi n/N} + w(n), \tag{4}$$

where h is the channel impulse response, τ is the time difference in samples between the transmitted and the received signal, $*$ denotes convolution, $\Delta\varphi$ is the corresponding CFO, and w is a zero-mean complex Additive White Gaussian Noise (AWGN) with variance σ_w^2.

The CFO is normalized with respect to the subcarrier spacing (Δ_f) and its value is assumed to span over the range $-0.5 < \Delta\varphi \leq 0.5$.

The frequency offset $\Delta\varphi$ may be also larger and can be divided into an integer and a fractional part. However, in the presence of an integer part the orthogonality between carriers is still preserved, given that the phase rotation introduced by the integer part can be easily compensated by a simple output rearrangement in the Fast Fourier Transform (FFT) and has absolutely no influence over the estimation of the fractional part. To this effect, the present analysis accounts only for the fractional part and assumes that the integer part is zero.

Furthermore, although the energy of the noise can be estimated in frequency domain, the SNR estimator is placed, in time-domain i.e. prior to the FFT. This is shown in figure in Fig. 1 and is particularly useful as it exhibits an early indication of the current SNR which enables the post-FFT stages to adapt quickly to the corresponding transmission conditions.

3 Algorithm Implementation

This section provides a systematic analysis of parameter-estimation techniques based on both the general case with infinite precision and SB-estimation. It is noted that the derivation of all algorithms assumes a static AWGN channel with no multi-path components. Therefore, the channel corresponds to a Kronecker delta function which is described by $h(n) \triangleq \delta(n)$. However, it is subsequently shown that the estimation functionality can be also extended to more realistic multi-path channels with low and moderate delay spread.

3.1 Full precision estimation

Time and Frequency estimation

A Maximum Likelihood (ML) estimator using a CP was proposed in [5] where the symbol timing (θ) and CFO ($\Delta\varphi$) estimates are determined based on the correlation between the CP and its counterpart in the OFDM symbol. The CFO is typically estimated more adequately in the time domain i.e., prior to the FFT operation [24]. An alternative, low-complexity method that is based only on maximum correlation was presented in [16] and is given by,

$$\hat{\zeta} = \arg\max_{n} \{|\gamma(n)|\}, \tag{5}$$

where

$$\gamma(n) = \sum_{k=n-L+1}^{n} \beta(k), \tag{6}$$

and

$$\beta(k) = r(k)\overline{r(k-N)}. \tag{7}$$

The over-line notation in (7) denotes the complex conjugation. Note that in fact (5) estimates the last sample in the OFDM symbol, given that the maximum correlation is typically found just after the full symbol has been processed. Based on this, it follows that the actual symbol start can be calculated by,

$$\hat{\theta}_l = \hat{\zeta} - N + 1, \tag{8}$$

or

$$\hat{\theta}_{l+1} = \hat{\zeta} + L + 1, \tag{9}$$

depending on whether the symbol timing is estimated in relation to the currently processed symbol, as in (8), or to the incoming symbol, as in (9). Since the real start of a symbol needs $\hat{\zeta}$ as reference, it can be straightforwardly claimed that symbol timing has been found once $\hat{\zeta}$ is estimated.

The CFO can be computed in two manners, namely, the peak-based frequency estimator and the angle-based frequency estimator. The former, which is considered in the present work, extracts the phase of the correlation peak vector and the estimator can be expressed as,

$$\widehat{\Delta\varphi}_p = \frac{1}{2\pi} \arg\gamma(\hat{\zeta}). \tag{10}$$

The latter extracts the average argument of the samples $\beta(k)$ with k placed in the CP. Thus, the CFO estimator becomes,

$$\widehat{\Delta\varphi}_a = \frac{1}{2\pi L} \sum_{k=\hat{\zeta}-L+1}^{\hat{\zeta}} \arg\beta(k). \tag{11}$$

The estimators in the current section are designed assuming infinite precision in the signal representation and they can be considered as conventional estimators. However, it will be shown in 3.2 that SB estimators are capable of maintaining performance degradation at reasonable levels with a significantly reduced complexity compared to the conventional estimators.

SNR estimation

It is recalled that the CP can also be used to estimate the noise in a received signal. It is also assuming that all communication anomalies have been compensated and that the only source of disturbance is AWGN and thus, i.e., $\tau = 0$, $h(n) = \delta(n)$, and $\Delta\varphi = 0$. As a result, the subtraction of each received sample from its counterpart within an OFDM symbol can be expressed as follows,

$$\begin{aligned} y(n) &= r(n) - r(n-N) \\ &= s(n) + w(n) - s(n-N) - w(n-N), \end{aligned} \tag{12}$$

where $s(n)$ and $w(n)$ denote the signal and noise sample components, respectively. To this effect, there are two cases to be considered: *i)* $s(n) = s(n-N)$, which holds when $s(n-N)$ is in the CP and $s(n)$ is at the end of the OFDM symbol; *ii)* $s(n) \neq s(n-N)$, which holds when the two samples belong to different OFDM symbols. This is illustrated in Fig. 2 where the first case corresponds to the positions enclosed within the dashed lines with lowest remaining energy. The amount of remaining energy within the dashed-lines is directly proportional to the noise power, since $s(n)$ and $s(n-N)$ in (12) cancel each other out, and can be thus used in SNR estimation.

Both the desired signal and the noise terms follow a complex Gaussian distribution. Therefore, $y(n)$ also follows a complex Gaussian distribution and its amplitude is Rayleigh distributed [30]. Hence, assuming $E[s(n)^2] = \sigma_s^2$, and $E[w(n)^2] = \sigma_w^2$, and taking into account the aforementioned possible cases, the corresponding variance becomes,

$$E[|y(n)_{\in \mathrm{CP}}|^2] = 2\sigma_w^2, \tag{13}$$

and

$$E[|y(n)_{\notin \mathrm{CP}}|^2] = 2(\sigma_s^2 + \sigma_w^2), \tag{14}$$

where the subscripts $_{\in \mathrm{CP}}$ and $_{\notin \mathrm{CP}}$ indicate whether n is within the CP or not. By combining (13) and (14), and approximating the expectation as an average over a suitable number of samples, the full precision SNR estimator can be expressed as follows,

$$\widehat{\mathrm{SNR}}_{\mathrm{FP}} = \frac{\sum |y_{\notin \mathrm{CP}}|^2}{\sum |y_{\in \mathrm{CP}}|^2} - 1, \tag{15}$$

The full precision SNR estimation technique compares the magnitude of pure-noise samples and noise-plus-signal samples for quantifying the respective SNR.

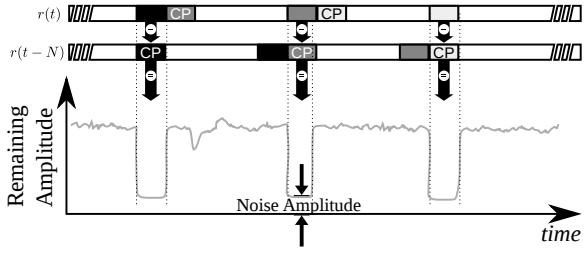

Fig. 2: Graphical representation of the signal subtraction $|y(n)|$ with channel $h(n) = \delta(n)$, $\tau = 0$, and $\Delta\varphi = 0$.

3.2 Sign-Bit estimation

In this section, the procedure of algorithm adaptation for SB estimation is detailed for the intended parameters as follows.

Sign-Bit time and frequency estimation

As already mentioned in Section 2, the correlation peak is used to determine the symbol timing. However, the considered signal in this case is now quantized to only the SB and thus (5), (6), and (7) can be expressed as,

$$\hat{\zeta}^q = \arg\max_n \{|\gamma^q(n)|\}, \tag{16}$$

$$\gamma^q(n) = \sum_{k=n-L+1}^{n} \beta^q(k), \tag{17}$$

and

$$\beta^q(k) = r^q(k)\overline{r^q(k-N)}, \tag{18}$$

where superscript q denotes that the received samples are quantized to the SB only. Consequently, the received sample takes only values $r^q(n) \in \{\pm 1 \pm i\}$, while the vector resulting from the complex multiplication in (18) has a phase with resolution of $\pi/2$, i.e., $\arg \beta^q$ takes only the values 0, $\pi/2$, π, and $3\pi/2$.

Analogous to full-precision, the frequency offset can be estimated in two ways subject to considerable advantages and disadvantages regarding the involved performance and complexity. In *peak-based frequency estimator* ($\widehat{\Delta\varphi}_p^q$), the estimate is extracted from the phase of $\gamma^q(\hat{\zeta}^q)$ yielding,

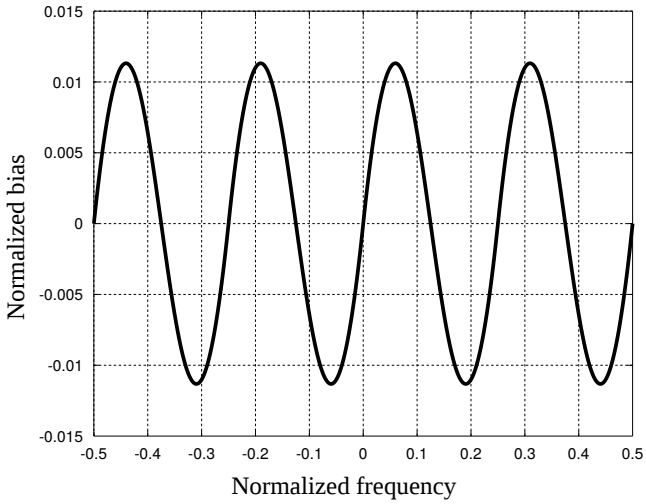

Fig. 3: Expected bias normalized to the subcarrier spacing, under noiseless conditions with non-dispersive channel.

$$\widehat{\Delta\varphi}_p^q = \frac{1}{2\pi}\arg\gamma^q(\hat{\zeta}^q), \tag{19}$$

where as before, $\hat{\zeta}^q$ is the estimated symbol timing and γ^q is the output of the correlator in (17). By initially assuming a non-dispersive noiseless scenario, i.e., $h(n)=\delta(n)$ and $w=0$, the bias[1] is illustrated in Fig. 3, where it is shown that its amplitude depends on the true fractional CFO. This bias is periodic in intervals 1/4 of subcarrier spacing, i.e., it is periodic in each quadrant of the complex plane. For the sake of simplicity, the analytical expression is derived for the first quadrant only ($0 \le \Delta\varphi < 1/4$), namely, [31],

$$E\left[\Delta\varphi_p^q\right] = \arctan\left[\frac{\Delta\varphi}{\pi/2-\Delta\varphi}\right]. \tag{20}$$

Each periodic interval possesses two maximum biases, positive and negative. They can be analytically deduced by (20). The maximum bias is at

$$\Delta\varphi = \left(\pi \pm \sqrt{-\pi^2+4\pi}\right)/8\pi \tag{21}$$

which results in approximately $\{0.06, 0.19\}$ and corresponds to $0.011 \approx 1\%$ of the normalized frequency in the noiseless scenario. It is noted here that although the bias is considered to affect the system performance, it is shown in Section 5 that under realistic communication scenarios, the loss incurred by the bias is practically negligible.

[1] Bias is defined as the difference between the estimator's expected value and the true value.

The second method of estimating the CFO, *Angle-based freq. estimator* ($\widehat{\Delta\varphi_a^q}$), consists of taking the phase of the individual samples within the CP. To this effect, the estimated value of $\Delta\varphi_a^q$ is computed as follows,

$$\widehat{\Delta\varphi_a^q} = \frac{1}{A}\sum_{A} \arg\beta^q_{\in \mathrm{CP}}, \tag{22}$$

where A is the number of samples used for the estimation. In most estimators, a large value of A improves estimation reliability by decreasing the estimation variance. However, this comes at a cost of longer latency as several symbols are used to obtain a single estimate. As a consequence, the processing time is increased.

In contrast to the peak-based SB estimator, the angle-based estimator is unbiased. This can be witnessed by assuming a noiseless environment with no multi-path components and considering, for simplicity, only the first quadrant of the complex plane i.e. $0 \leq \Delta\varphi < 1/4$. Under this assumption the argument of β^q can only be 0 or $\pi/2$ whereas the probability that $r^q(n)$ and $r^q(n-N)$ have different phase is given by,

$$P\{\arg\beta^q(k) = \pi/2\} = \frac{\Delta\varphi}{\pi/2}. \tag{23}$$

Based on this, the expected value of the estimator can be expressed as follows,

$$E[\widehat{\Delta\varphi_a^q}] = \frac{\pi}{2}P\{\arg\beta^q(k) = \pi/2\} = \Delta\varphi. \tag{24}$$

At first glance the angle-based ($\widehat{\Delta\varphi^q}_a$) seems a better alternative since it is unbiased. Nevertheless, it is extensively shown in Section 5 that its performance is affected substantially more by the delay spread compared to the case for peak-based ($\widehat{\Delta\varphi^q}_p$).

Sign-Bit SNR estimation

Another application of SB estimation in OFDM systems is low complexity SNR estimation based on the CP. Under the assumption that the only source of disturbance between transmitter and receiver is AWGN, i.e., the same initial scenario as defined for full-precision, the results from subtracting each receiver sample from its counterpart in the CP is expressed as,

$$y^q(n) = r^q(n) - r^q(n-N). \tag{25}$$

Intuitively, if the noise power is small in comparison to the signal power, the sign of the received sample in the CP is the same as its counterpart within the symbol, resulting in $y^q(n) = 0$. However, as the noise power grows, there is an increased risk that the sample in the CP has the opposite sign than in the OFDM symbol and consequently the result of the subtraction yields $y^q(n) \neq 0$ probabilistically. This is illustrated in detail in Fig. 4 which shows curves of the probability density function (PDF) of the real part (the same analysis applies for the imaginary part) of the received signal at samples $r(n)$ and $r(n-N)$, which correspond to the CP and its counterpart in the symbol, respectively. The darker rings indicate higher probability density, while it is also noted that the number of rings and its density are a function of the noise variance. The center of the probability density function is located at the noiseless sample $[s(n), s(n)]$. The dashed line depicts all possible cases where $s(n) = s(n-N)$ with slope equal to unity. Therefore, the probability density of the received sample is always centered on the dashed line.

Next, consider the case in Fig. 4 where the received noiseless signal is positive and the noise density expands along the four quadrants, e.g., any ring of the probability density function that occupies all quadrants. It is graphically shown that when subtracting $r^q(n)$

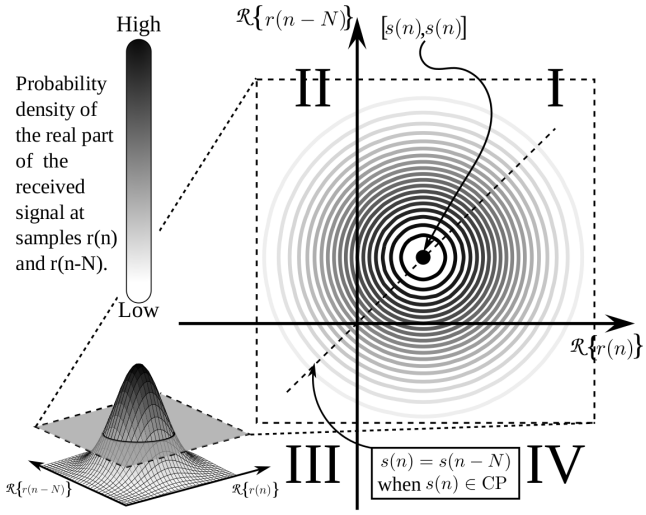

Fig. 4: Level curves of the real part of the received signal density at samples $r(n)$ and $r(n-N)$ with the four quadrants indicating the sign of the received sample. The samples $r(n)$ and $r(n-N)$ are in the CP and its counter-part in the symbol, respectively, the same is valid for the imaginary part.

from $r^q(n-N)$, the resulting sign lies within one of the four possible quadrants. The quadrants describe the following four states: *i*) when no sign change takes effect (I); *ii*)when only the sign of the $r(n)$ is changed (II); *iii*) when the both signs are changed (III); *iv* when only the sign of the $r(n-N)$ is changed (IV). It is noted here that it is impossible to practically distinguish between I and III, since the result of the subtraction yields the same outcome. Likewise, by considering only cases II and IV it is possible to describe the probability density that the subtraction will yield a value different than zero. Hence, the corresponding probability density is expressed according to [32], namely,

$$\begin{aligned} p = &\frac{4}{\sqrt{2\pi}} \int_0^{\infty} Q\left(\frac{s}{\sigma_w}\right) \exp\left(-\frac{1}{2}s^2\right) ds \\ &- \frac{2}{\sqrt{2\pi}} \int_0^{\infty} Q^2\left(\frac{s}{\sigma_w}\right) \exp\left(-\frac{1}{2}s^2\right) ds, \end{aligned} \tag{26}$$

where s denotes the transmitted sample and σ_w is the standard deviation of the AWGN. Using [4], [21] and after some mathematical manipulations, the SNR and p are linked by $\widehat{\mathrm{SNR}}_{SB} = 1+\cos(\pi p)/\sin^2(\pi p)$. The value of p is approximated by averaging enough number of samples $|y^q_{\in \mathrm{CP}}|$ so that a reliable SNR estimate can be computed. Notably, even though the presented analysis considers only the AWGN scenario, it is subsequently shown that SB estimation goes beyond this condition. Moreover, the advantages offered by these techniques when decreasing the corresponding hardware complexity are presented extensively.

4 Hardware Implementation

In order to ensure consistency with performance evaluations, an equivalent architecture with an 8-Bit resolution is created and compared to the SB architecture. This is illustrated in

Fig. 5, where white blocks are considered external and irrelevant to the complexity analysis. The dashed line in figure, and in subsequent architectural diagrams, represents the path where a single real value is passed. On the contrary, the solid lines represent I and Q components i.e., two values, passing between the blocks. A more detailed description of each architecture is additionally depicted in figures 6 and 7. Importantly, both architectures can estimate the peak-based CFO using the external arctan module which is typically implemented with a COordinate Rotation DIgital Computer (CORDIC) [29] [18] in Fig. 5. However, only the SB-architecture appears to be capable of estimating the angle-based and peak-based CFO. This is due to the much higher complexity requirements that the angle-based CFO imposes when the signal is quantized to 8-bits with no performance benefits, in comparison with the already available 8-bit peak-based estimation.

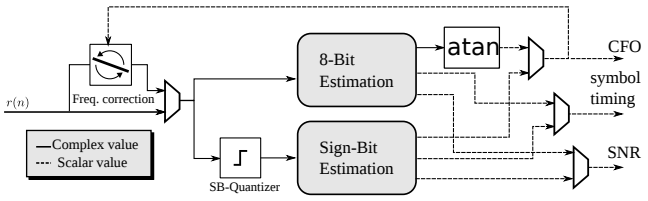

Fig. 5: Complexity analysis conceptual image, where frequency-correction, SB-quantizer, arctangent, and multiplexers, are considered external and outside the complexity analysis.

4.1 8-Bit architecture

The architecture depicted in Fig. 6 is capable of estimating the intended parameters based on the methodology introduced in Section 2, when its input signal is quantized to 8 bits. Its operation is based in two modes: firstly, the *time-frequency* mode is in charge of performing initial time and prepares the signal for CFO estimation; and secondly, the *SNR* mode is in charge of performing SNR estimation. Since the *SNR* mode requires input from the time-frequency, the modes are mutually exclusive and can share some hardware components.

Time-Frequency Mode

In this mode the correlation peak is calculated by multiplying the input signal with its conjugate version delayed by N samples and subsequently adding the previous A multiplications - see equations (6) and (7). This is realized in hardware by the combination of a First Input First Output (FIFO) memory and a complex multiplier, that calculate the value of $\beta(n)$ at each sample. Subsequently, two moving-sums add the last A multiplication results for I and Q, respectively.

The symbol timing according to equation (5) is estimated as the position (in samples) where the correlation is maximum. As a result, a Finite State Machine (FSM) is used for keeping track of the correlation output. It is recalled here that the correlation value is a complex quantity and as a consequence, its absolute value needs to be computed in order to test for maximum amplitude.

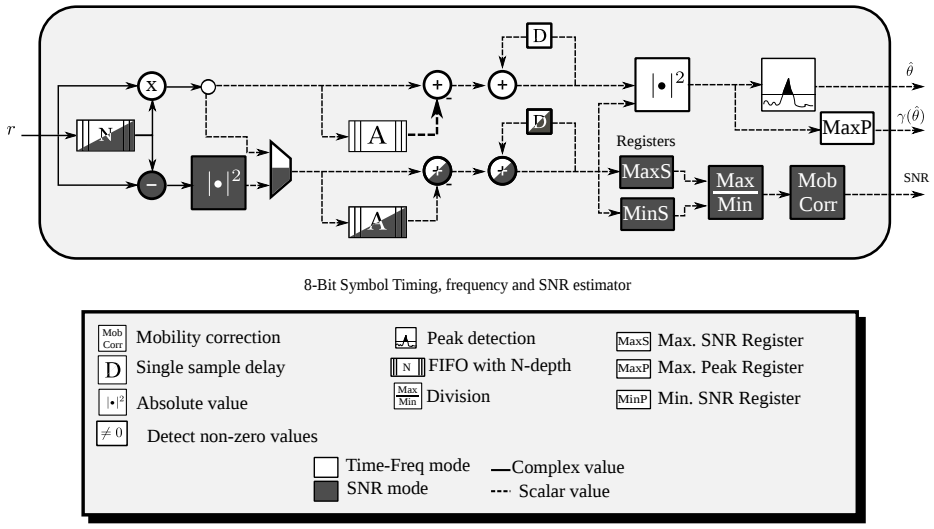

Fig. 6: Block diagram of architecture of 8-Bit, capable of estimating symbol timing, CFO and SNR. The dark modules are used for SNR estimation, the white for time-frequency and the mix-colored for both.

SNR Mode

In this mode the SNR is estimated by approximating the amount of energy within the CP and outside the CP. This is accomplished in hardware by subtracting the input signal from its delayed version. For the delay, the same FIFO memory as in the *time-frequency* mode can be used, whereas the subtraction and the posterior energy calculation is done by a 8-bit subtraction and an absolute-value module that squares the result of the subtraction and averages both I and Q components.

One of the two available moving sums, the bottom one from Fig. 6 in the architecture, can be used for adding the amount of energy within the CP length. The FSM also ensures that the amount of energy corresponding to the energy inside and energy outside the CP is stored in the registers MinS and MaxS, respectively. The SNR is then realized by computing the ratio between MaxS and MinS. The ratio is implemented as a sequential divider that converges in several clock cycles. A correction is then applied to the calculation to account for multi-path channels, this is discussed in Section 5.2.

4.2 Sign-Bit architecture

Analogous to the 8-bit architecture, the SB architecture, depicted in Fig. 7 can estimate the same parameters while it can additionally provide the angle-based CFO. Furthermore, it operates in the same two modes; first time-frequency and SNR modes, executed in that order. It can also be noticed that the SB architecture has considerably fewer elements than its higher precision counterpart. Additionally, the majority of the elements can be fully shared between the two operational modes.

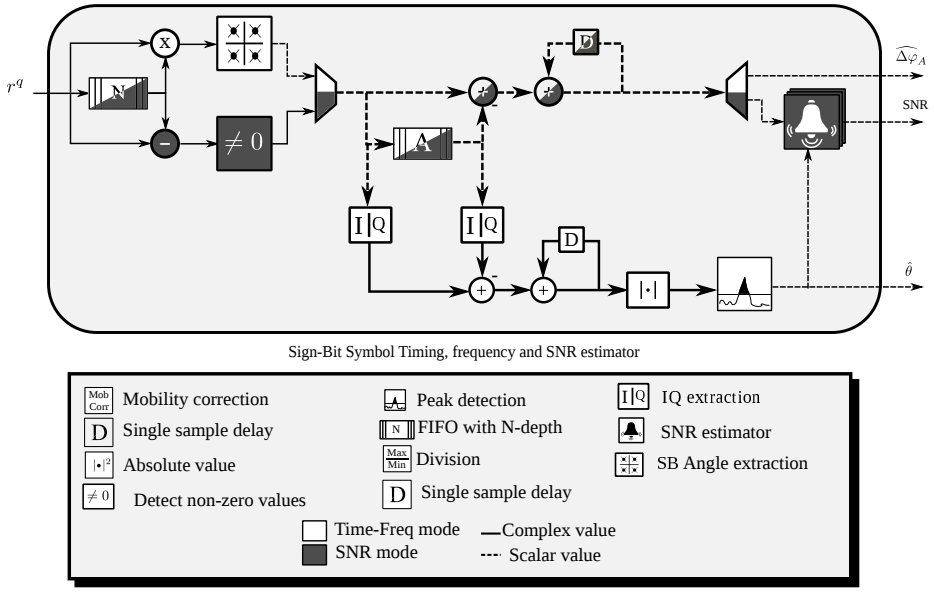

Fig. 7: Block diagram of SB hardware architecture, capable of estimating symbol timing, CFO and SNR. The dark modules are used for SNR estimation, the white for time-frequency and the mix-colored for both.

Time-Frequency Mode

Due to the heavy quantization, strength reduction[2] plays an important role in reducing the corresponding hardware complexity. The size of the FIFO is reduced dramatically while the multiplication becomes a single xor-boolean operation. In addition, a complex CORDIC architecture can be avoided when extracting the phase of β in (22), since the phase can only take four possible angles, namely, $0, \pi/2, \pi$, or $-\pi/2$. The moving-sum is also simplified since it is not necessary to keep two separate moving-sums for I and Q components as these components can be straightforwardly extracted from the angle itself.

Similar to the 8-bit architecture, the peak detection module is an FSM that monitors the value of $|\gamma^q(n)|$ for the previous 2 symbols and determines the location of the corresponding maximum. The FSM then reports this position as the symbol timing estimation $\hat{\zeta}$.

The architecture for time-frequency only was presented in [13] and was later fabricated in a CMOS 65 nm process with the layout illustrated in Fig. 8. The measurements from the fabricated SB-time-frequency-correlator are shown in Fig. 9, where the red and blue color correspond to the simulated and measured CFOs respectively ($\widehat{\Delta\varphi_a^q}$). Likewise, the cyan and magenta curves correspond to the simulated and measured correlation peak, respectively. They both show a distinctive peak corresponding to the position where the symbol-timing ($\hat{\zeta}$) is located. It is noted that the slight difference between simulation results and measurements results occurs for two reasons: firstly, an initialization phase when the FIFOs are being filled most noticeable in the CFO); secondly, a sample offset between the simulation and the measurements. It is also shown that the measurements report an average power dissipation

[2] Strength reduction is a known optimization technique where complex operations are replaced by equivalent but simpler and less expensive operations [11].

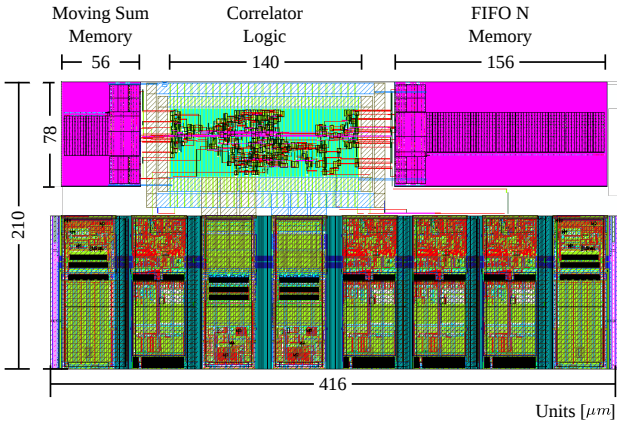

Fig. 8: Fabricated SB-time-freq-correlator in ST 65 nm Technology with High VT low power cells.

of 0.62 mW for LTE, with 20 MHz bandwidth, with a power supply applied to the core of 1.2 V.

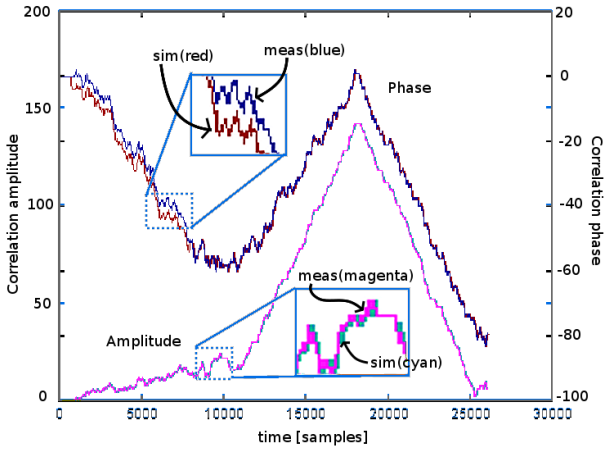

Fig. 9: Measured Peak and Angle compared to Matlab^{TM}simulations. The CFO estimation red and blue correspond to the simulated and measured, respectively. While $|\gamma^{\prime}(n)|$ is represented with cyan and magenta for simulated and measured, respectively. The horizontal axis represent number of samples and the vertical axes a integer number relative to the actual value of the corresponding parameter.

SNR Mode

In this mode, the incoming signal is assumed to be CFO-clean, i.e., symbol-timing and CFO correction have been performed in the previous mode. The sign of the input signal is subtracted from its delayed version with the aid of the same FIFO used in *time-frequency* mode

Table 1: 3GPP channel models with its corresponding Doppler shift and delay spread [1].

Channel Model	Maximum Doppler Shift	RMS Delay Spread
Extended Pedestrian A (EPA)	5 Hz	43 ns
Extended Vehicular A (EVA)	5 Hz	357 ns
Extended Typical Urban (ETU)	70 Hz	991 ns

for correlation. The block named non-zero detector counts the number of received samples that had changed sign[3] and inputs this value to the moving-sum. Notably, the same moving-sum used for the *time-frequency* mode. The SNR is then estimated by inserting the total number of flipped signs to the estimation tile, as depicted in Fig. 7 with a bell icon, and implemented as a Look-Up Table (LUT). The LUT extracts the SNR based on the corresponding probability p. Since p varies in relation to the current channel, the architecture contains an estimation tile LUT per channel model.

5 LTE Performance trade-offs

The analysis presented in the current study applies to any OFDM system. However, in order to evaluate the proposed methods in a realistic manner, the LTE communication standard is chosen as the target application. LTE has been developed by the 3GPP in its release 8 and defines a basic sample rate of 30.72 MHz for the maximum component carrier bandwidth of 20 MHz with a sub-carrier spacing of 15 kHz [2]. The size of the FFT is 2048. In LTE there is a normal and an extended CP with durations of 4.7 μs and 17 μs, respectively (equivalent to 144 and 522 samples). The normal CP is the most commonly used mode and thus, selected in the present analysis. Performance evaluation is carried out by Matlab simulations with channel characteristics described in more detail by [1] under 20 MHz bandwidth subject to Rayleigh fading. It is recalled that 3GPP provides three reference channel models of typical multi-path propagation environments summarized in Table 1. Furthermore, the proposed analyses are compared to a more conventional yet equal estimation where the signal is quantized to 8-bits. In what follows, the same 8-bit methods are also used for corresponding complexity analysis and comparisons.

5.1 Sign-Bit time and frequency estimation under LTE specifics

In OFDM systems, time and frequency estimation are typically considered as a joint estimation process given that frequency estimation cannot be performed prior to time estimation. However, in this section they are presented separately in order to analyze their performance individually.

5.1.1 SB Time estimation

It is recalled that estimating the exact symbol start is not particularly crucial in OFDM systems. In order to avoid Inter-Symbol-Interference (ISI), it is sufficient if the estimated

[3] A change of sign is perceived as a non-zero result from the subtraction (See Sect. 3.2)

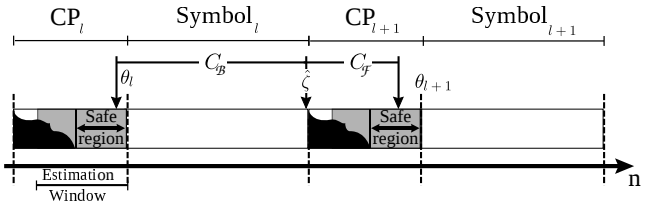

Fig. 10: Graphical representation of the safe region, the estimation window, and their relation to the channel impulse response.

symbol start lies anywhere within the end of the channel impulse response and the end of the CP, which is denoted as safe region in Fig. 10. However, some performance analysis can be carried out based on the statistics of the estimator. To this end, it is firstly assumed that a symbol l and its corresponding CP are used for the time estimation; since the symbol plus the CP have a total of $N+L$ samples, the symbol timing is expected to be found at position $\hat{\zeta} = \theta_l + N - 1$ (see Fig. 10). Consequently, a positive/negative constant (C_F or C_B) can be safely added in order to reposition the $\hat{\theta}$ closer to the center of the safe region, allowing timing errors in both directions. The estimation window is the region where samples are taken from in order to perform the corresponding estimation. The ideal case with the most reliable estimation would be if the estimation window covers only the safe region (See Fig. 10). However, in the presence of multi-path components, the length of the safe region varies with each channel realization while the estimation window remains constant. Thus, introducing 'unclean' samples into the estimation. i.e., samples affected by the channel impulse response. As a consequence, the channel introduces an offset which is dependent upon the rms delay spread. Fig. 11 shows the average estimated symbol timing ($\hat{\zeta}$) for the EPA, EVA, and ETU. The symbol-timing appears as a positive shift from the expected symbol timing when no delay spread is present i.e., in the case of a Rayleigh flat fading channel.

Observing any of the curves for one channel model in Fig. 11, it is noticed that the difference between SB and 8-bit average symbol-timing is practically zero for SNR higher than 4 dB i.e., only a fraction of a sample. However, this is not the case for SNR lower than 4 dB due to the higher quantization in the SB method. This is demonstrated more clearly in the figure at 0 dB SNR, where the quantization noise dominates the estimator's statistics. Based on this, the three channel models have similar average estimated value, regardless of the different value of rms delay spread. Moreover, the distance from the expected to the estimated value is quite small compared to 144, which is the length of CP for LTE. The corresponding standard deviation is shown in Fig. 12 and, as expected, it decreases as the SNR increases, with minimum deviation of 2 samples above 16 dB SNR. It is also noted that the cross-over points mark the limit where SB matches or slightly out-performs the 8-bit precision in terms of standard deviation due to the heavy quantization. At high SNR the quantization rejects small impurities, i.e., the signal becomes more distinct, which results in a well-defined autocorrelation peak. Note also that, since at high SNR the noise is in any case already small, the SB out-performs the 8-bit by a couple of samples only, which compared to 144 is negligible. Thus, one may conclude that the performance of symbol timing estimation is virtually the same for both 8-bit and SB.

In the high SNR regime, the SB appears to have better performance than the 8-bit counterpart. This is because the sign-bit quantization removes all small variations from the received signal -the noise amplitude is much smaller than the transmitted signal amplitude- resulting in a more distinctive correlation peak i.e. smaller variance, for SB in comparison

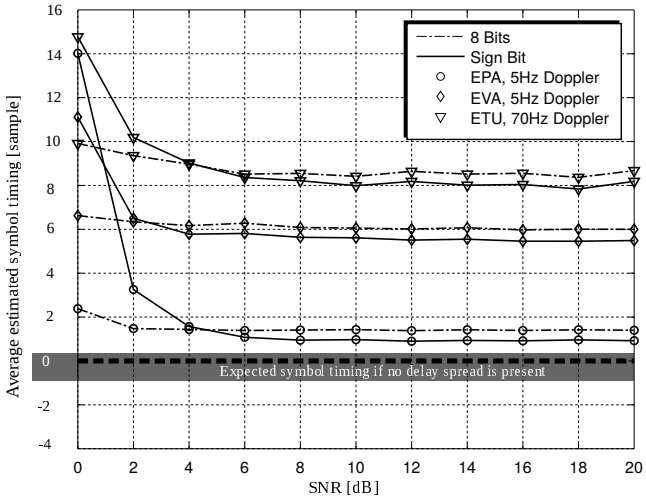

Fig. 11: Estimated Symbol timing for EPA, EVA and ETU channel models, relative to that expected symbol timing under none multi-path environment.

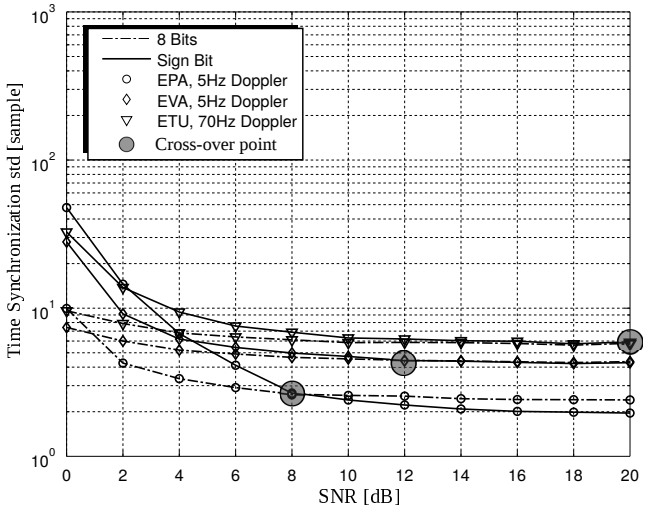

Fig. 12: Symbol timing standard deviation for EPA, EVA and ETU channel models as a function of SNR.

to 8-bit. However, in the low SNR regime the opposite holds since the quantization removes a large portion of the signal in the SB method. It is also expected that the standard deviation increases with the channel's rms delay spread, since in a multi-path environment the channel impulse response affects samples in the estimation window. The correlation function $\gamma^A(n)$ in (17) is not capable to disregard samples affected by the channel, hence, the larger the delay spread, the more samples are affected and thus, the larger the standard deviation. This appears to affect both SB and 8-bit methods with the difference in standard deviation for the various channel models.

5.1.2 SB frequency estimation

CFO appears at the receiver as a consequence of frequency mismatch at the local oscillators and Doppler shift due to relative motion between transmitted and receiver. Given the channel models introduced in section 5, the maximum Doppler shift considered is 70 Hz, which is considerably small compared to Δ_f, and does not represent a hindrance to the system. However, the maximum CFO due to oscillator mismatch is much larger and needs appropriate compensation, i.e., it equals 53.75 KHz$\approx$3.5Δ_f[4]. Also recall from section 2 that this CFO is divided in an integer and a fractional part, where the presented estimator operates over the fractional part only, whereas the integer part is compensated at subsequent stages of the receiver.

As phase information of each sample is lost due to quantization, it is reasonable to expect that SB frequency offset estimation would perform worse than higher precision. Nevertheless, it is more relevant to determine whether the corresponding performance loss is significant or not.

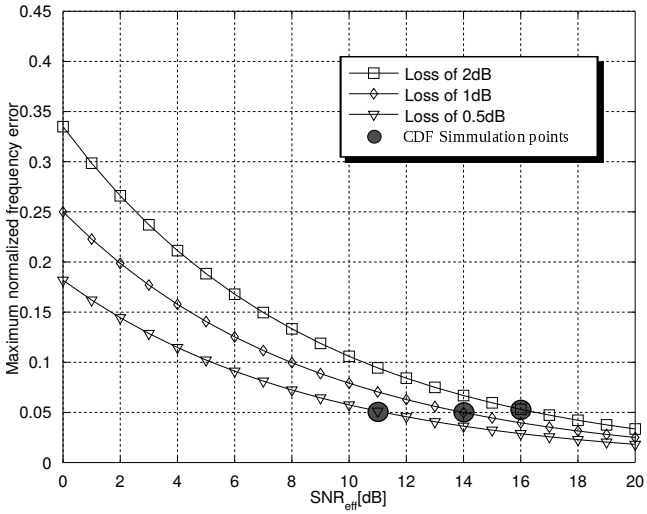

Fig. 13: Maximum allowed fractional frequency error normalized to the subcarrier spacing (Δ_f =15 kHz) for a allowed loss of: from top to bottom 2dB, 1dB, and 0.5dB due to ICI interference.

After estimating the CFO, the received samples have to be compensated in order to restore orthogonality in the frequency domain. If the estimation is not accurate, the compensation is not able to completely eliminate the CFO and the impact of the remaining offset can be measured by the introduced ICI. For a low CFO relative to the subcarrier spacing (Δ_f =15 kHz), the ICI power can be approximated as [25]

$$I = \frac{\pi^2}{3}(\Delta\varphi)^2. \tag{27}$$

By treating I as additional noise, the effective SNR becomes

[4] Considering a typical crystal accuracy of $\pm$20 ppm [15], and 5 MHz transmission bandwidth at the edge of the band 41 available in USA [12].

$$\mathrm{SNR}_{eff} = \frac{S}{\eta + I}, \tag{28}$$

where η is the noise introduced by the channel and other imperfections, and S is the power of the desired signal. Fig. 13 illustrates the maximum allowed fractional frequency offset, normalized to subcarrier spacing, so that there is a respective maximum SNR loss of 2 dB, 1 dB and 0.5 dB due to the remaining frequency offset in the system. To measure the performance of the estimator, take for example, a maximum allowed frequency error of 0.05 with SNR_{eff} of 16 dB, 14 dB and 11 dB, corresponding to CDF simulation points in Fig. 13. Then, Fig. 14 shows that the probability of the frequency offset is smaller than 0.05 for SB estimation lies between 0.6 and 0.8. Hence, it becomes clear that higher precision (8 Bits) performs better, with probability larger than 0.9, in all simulated cases.

The channel estimation suffers a performance degradation due to the remaining frequency error. In order to quantify this degradation, Bit Error Rate (BER) simulations where performed for an LTE uncoded Single Input Single Output (SISO) channel under 20 MHz transmission bandwidth. The simulations are shown in Fig. 15 with normalized frequency error of 0, 0.05 and 0.1. By observing the corresponding figure, it is noticed that the loss due to frequency error is negligible.

The precision of the SB estimator can be improved by averaging. However, this comes at the cost of increasing latency and consequently energy consumption, as the estimator needs to process multiple symbols in order to produce a single estimate. This is shown in Fig. 16 where the estimator performance for 8-bits using one symbol is compared to SB for various number of symbols.

It is also worth noticing that LTE contains specific Primary Synchronization Signals (PSS) intended for time synchronization and acquisition of base-station ID. These signals are pseudo-random sequences transmitted in intervals of 0.5 ms [23]. SB estimation can also be used to estimate time and frequency in such sequences as it is demonstrated in [28]. However, in the current analysis the CP is used as means of synchronization in order to demonstrate the generalization to any OFDM system.

5.2 Sign-Bit SNR estimation under LTE specifications

A mobile terminal pursues the best possible connectivity by continuously seeking a base-station with better transmission conditions. Since the mobile terminal is already connected to the network while searching for other base-stations, some properties of the environment are unchanged during the transition, since the terrain cannot change instantly. Therefore, it is possible to assume some knowledge of the currently most suitable channel model.

The average estimated SNR is depicted in Fig. 17 where a bias is observed in both methods, distance between the mean and the ideal value, but is more significant in the 8-bit estimation. The bias results from the channel's impulse response affecting samples in the CP. Hence, the larger the channel delay spread, the more samples are affected and thus, the larger the corresponding bias. This is noticed in the figure by comparing for any method, either 8-bit or SB EPA with the shortest, and ETU with the longest delay spreads. The estimated value is the closest to the ideal in EPA and most distant from it in ETU channel model.

Samples distorted by the channel impulse response affect the performance of the SB only by its sign, not by its amplitude, contrary to the 8-bit method. Thus, it can be graphically deduced that for any channel model, the bias in the SB method is smaller than the 8-bit.

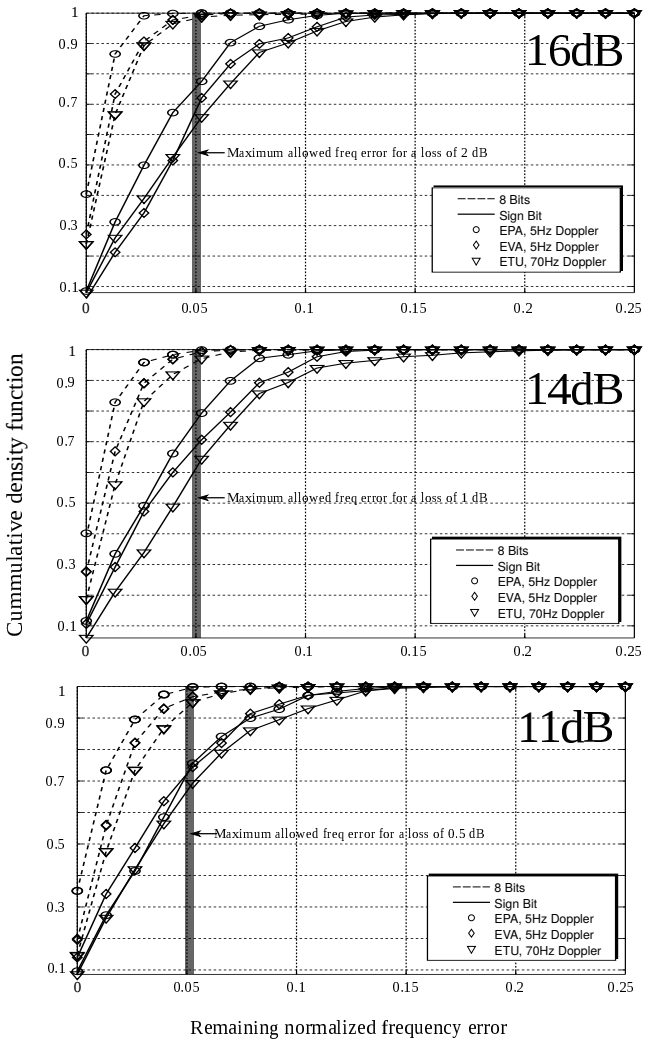

Fig. 14: Cummulative density function of maximum allowed fractional frequency error normalized to the subcarrier spacing (Δ_f =15 kHz) for SNR$_{eff}$ of: 16, 14, and 11 dB.

Furthermore, it is possible to combat the channel dependent bias by decreasing the size of the moving sum and consequently reducing the number of samples introduced to the estimation window that were affected by the channel impulse response. However, this in turn increases the estimator's variance, which affects its performance.

Another way to remove the bias is to characterize it statistically for each method and each channel model and then compensate the estimation accordingly. This can be possible under the assumption that some knowledge of the channel properties exists. The results of this compensation are depicted in Fig. 18 with the mean and 5%-95% confidence intervals of the estimation methods. The region with solid lines corresponds to SB estimation while the region with the dashed lines corresponds to 8-bits estimation for EPA, EVA and ETU. The centered line represents the mean value after compensation and the envelope around it

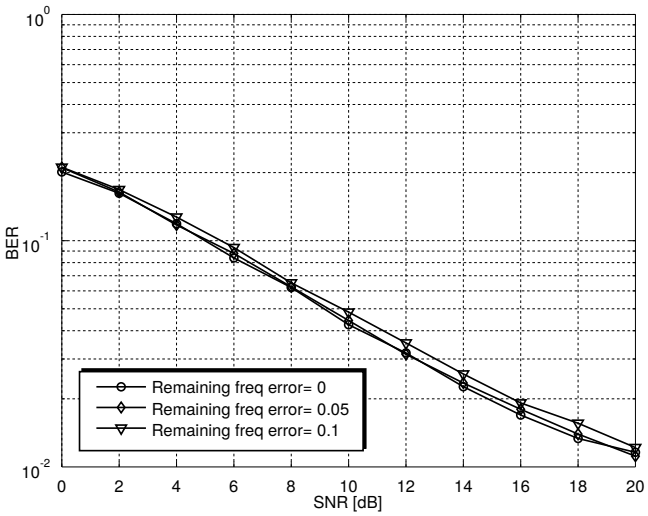

Fig. 15: BER for a LTE SISO with 20 MHz bandwidth, QPSK modulation uncoded transmission with normalized frequency error equivalent to 0, 0.05 and 0.1

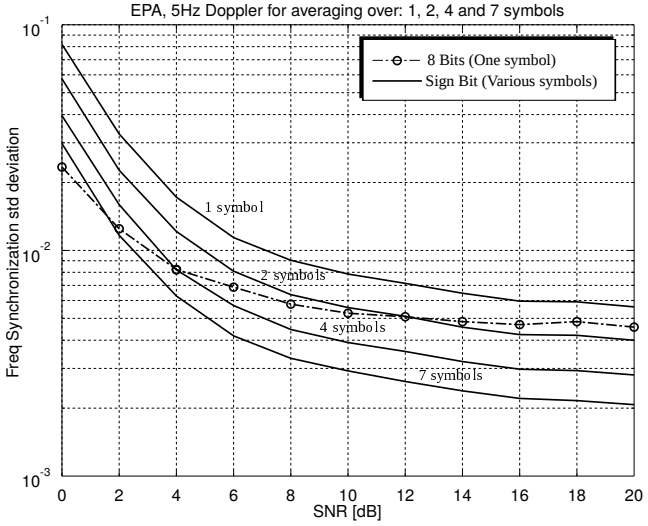

Fig. 16: Frequency estimation standard deviation and improved standard deviation for SB-estimation.

denotes its confidence interval. From the figure, it can be seen that for all channel models the 8-bit has the smallest variance - approximately ± 2 dB. The variance of SB is slightly larger than the 8-bit one in most cases with the worst case scenario being EPA, with a variance of ± 4 dB at true SNR of 16 dB. The figure depicts the result of simulations performed with 21 OFDM symbols to create a single estimate, the variance -or confidence interval- can be reduced for this worst case by increasing the number of symbol used per estimate, at the cost of increasing estimation latency. It is noted here that compensation for SB has much lower complexity in terms of hardware compared to the 8-bit. This is achieved because

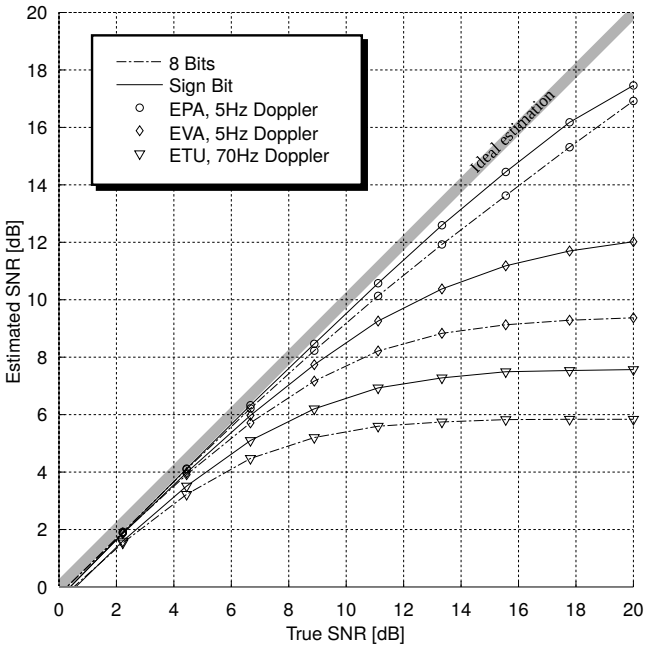

Fig. 17: Average estimated SNR uncompensated simulated for EPA, EVA, ETU, and AWGN channel models. Each estimation is realized as an average of 21 consecutive OFDM symbols with a moving sum size of 115 samples.

the SB-SNR compensation requires only one LUT per channel model, whereas 8-bit-SNR compensation needs one LUT per channel model with higher resolution, in addition to a division module, which is typically a costly operation in hardware systems.

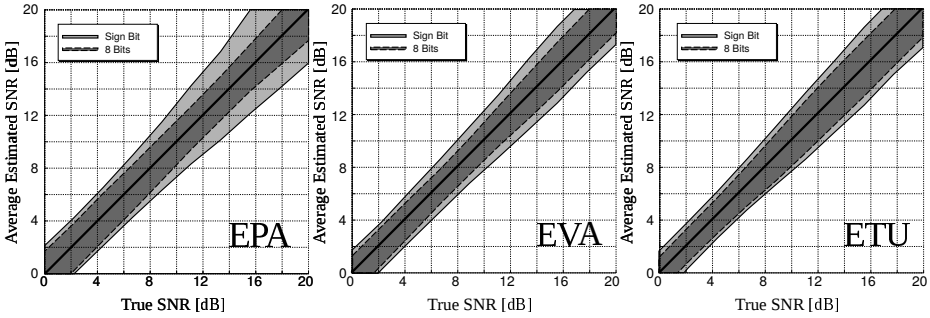

Fig. 18: Estimated SNR with 5% - 95% confidence intervals, compensated for channels EPA, EVA and ETU. Each estimation is realized as an average of 21 consecutive OFDM symbols with a moving sum size of 115 samples.

So far, the received signal used for SNR estimation is assumed to have no CFO, which requires perfect CFO compensation. In this case the remaining frequency error affects the SNR estimation. This is illustrated in Fig. 19, where it can be seen that the estimated SNR

deviates from the true SNR when there is any CFO remaining in the signal. As an example, when the remaining normalized frequency error is 0.05, according to Fig. 14, the probability of the error being smaller than 0.05 for an SNR_{eff}=11 dB is larger than 70% for all cases. This implies that even in the presence of a remaining frequency error in the SNR estimation, this rarely reaches a value that can severely affect SNR estimation.

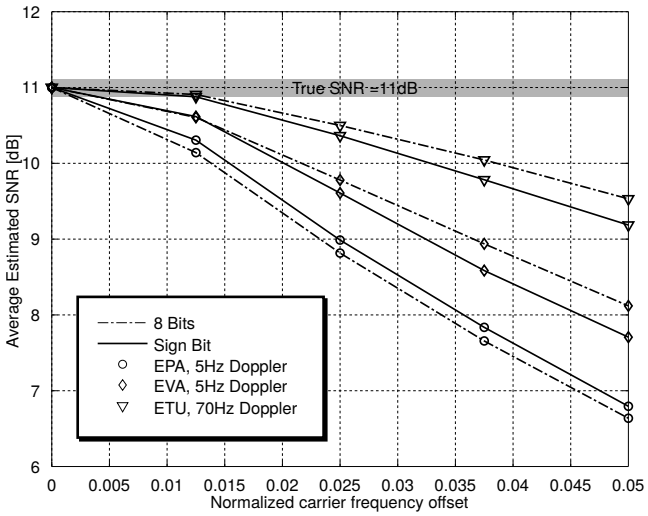

Fig. 19: Effect of remaining CFO into SNR estimation for EPA; the CFO is normalized to the subcarrrier spacing (15K Hz).

In this section the performance evaluation of SB estimation techniques have been presented in the context of an LTE receiver with realistic channel models. From the simulations, it can be concluded that the SB estimation has similar performance to 8-bit, for symbol timing and SNR. Notably, the CFO estimation, even though the SB estimation performance is worse than 8-bit, it rarely appears to be harmful enough for the subsequent tasks in the receiver.

In the following section, the low complexity implementation of SB estimation is addressed by describing an architecture that can reuse hardware and compute the SB-estimates.

6 Complexity trade-offs

In order to obtain a clear idea of the complexity trade-offs associated with the SB estimation, the SB architecture and its equivalent higher precision counterpart are compared to eachother along with relevant existing techniques for estimating symbol-timing and CFO. The top-level architecture previously described is synthesized, placed, routed and simulated to extract area and power numbers, the top-level layout is shown in Fig. 20. It is noted here that the estimation principle can be applied to any OFDM system, which is demonstrated by designing a rather scalable combined architecture so that it can be conveniently employed in three OFDM standards, namely, IEEE 802.11 (WLAN), Digital Video Broadcasting - Handheld (DVB-H) in 4K mode, and LTE. The synthesis results for both SB and 8-bit are

depicted in Fig. 21 with the total area and power consumption split into memory and logic contribution.

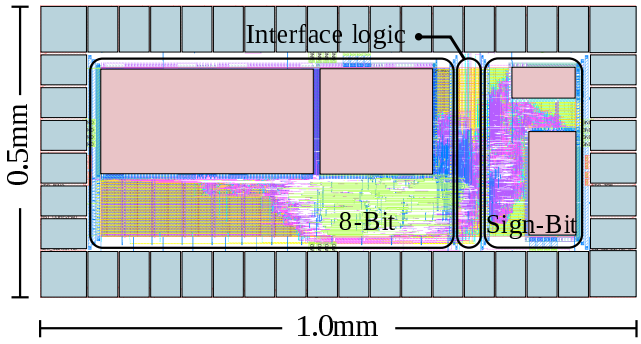

Fig. 20: Fabricated SB-time-freq-correlator in ST 65 nm Technology with High VT low power cells.

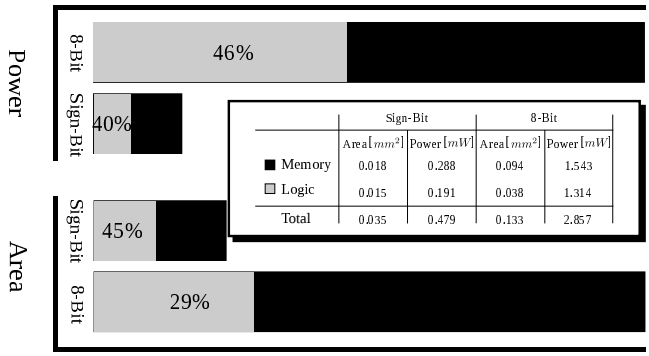

Fig. 21: Power and area distributions for SB and 8-bit after place and route. Post-layout simulation performed with LTE 20MHz bandwidth and fully-back annotated simulation at 1.2V supply

It can be seen that the total area of the 8-bit architecture is 4 times larger than it's SB equivalent and dissipates 6 times more power. Even though one could expect the 8-bit area overhead to be at least 8 times larger, this is not the case due to the fact that larger memories, in terms of storage, are typically denser. For example, the memory in the 8-bit architecture used for correlation (the largest in the design) has an area density of 0.9μm^2-per-bit for the 8-bit architecture, which is almost a factor of 2 denser than the SB memory with 1.6μm^2-per-bit.

In the SB architecture, the logic, which occupies 45% of the total area, dissipates 40% of the total power which implies that the power and area are memory dominant. Likewise, in the 8-bit architecture, the logic occupies 29% and dissipates 46% of the total energy. The simulated leakage was excluded from the figure since, according to post-layout simulations, it only accounts for 0.04% and 0.03% of the total dissipated power for SB and 8-bit, respectively.

In order to see what other logic modules can be meaningful contributors, a further partition into individual hardware blocks is shown in Table 2. Recall that the SNR is calculated

Table 2: Area and Power breakdown of the various parts of the architecture.

	8-Bit [%]		Sign-Bit [%]	
	Area	Power	Area	Power
Correlation FIFO	49	32	45	42
Moving Sum FIFO	34	45	28	37
Register Bank	6	2	14	6
Peak detection	2	0.67	6	4
Complex multiplier	3	9.7	-	-
SB Complex mult + angle extraction	-	-	0.5	1
SNR Est. (divider + comp.)	4.06	1.101	-	-
SNR Est. (LUT)	-	-	2	0.01
Remaining logic	2.3	9	4	10.5

differently in both methods, i.e., in the case of the 8-bit architecture, a block to perform sequential division is used (See Section 3.1), and in the case of SB a LUT is used to extract the SNR estimation based on the statistics of the signal subtraction (See Sections 3.2 and 5.2). In both architectures the largest area/power contributors are the modules containing memories. The third most important contributor is a register bank used to store intermediate and final values. This accounts for 14% of area with 6% of the power for the SB and 6% of area with 2% of the power for the 8-bit architecture. It is also noted that the contribution of the correlation FIFO and the moving sum FIFO adds up to a share larger than the one reported in Fig. 21. In order to avoid using area expensive dual-port memories to perform FIFO functionality, a much more compact single-port, surrounded by extra logic needed to emulate a FIFO, is alternatively used. Furthermore, the moving sum is a combination of a FIFO, arithmetic elements and registers. Thus, each FIFO implementation accounts for more than just memory elements.

Table 3 shows the comparison of the proposed architecture to other designs found in literature. It is worth mentioning that [6], [27] and [7] are designed for time-frequency synchronization of WLAN where there is a synchronization preamble. In the WLAN legacy version, the preamble is a predefined sequence consisting of 10 short symbols of 16 samples each, with their values being specifically designed to provide a high correlation peak. The proposed architecture can be used for WLAN, but it was intentionally designed to support more memory demanding standards such as LTE and DVB-H. Thus, a downsized version of the architecture is used for fair comparison, i.e., the FIFO is reduced from 4096 words to 16 and the memory in the moving sum is reduced from 512 to 160 words. For LTE and DVB-H the size of the largest FIFO is the size of its corresponding FFT, which is 2048 and 4096 respectively, whereas in WLAN, the same FIFO is reduced to the size of a short training symbol in the preamble with size 16. It is also seen in Table 3 that both architectures have a smaller gate-count and power consumption than previously published works, regardless of the extra-functionality. Furthermore, the SB architecture can reduce the area and power to a tiny fraction of those reported in literature. Besides being more power and area efficient, both architectures provide a coarse SNR estimation that can improve energy efficiency even further, by providing an early channel prediction in later stages. It is worthwhile to mention that the comparison is made with other works using very different algorithms. Where in many cases, estimation performance was the ultimate goal, whereas in this work the authors trade-off performance for area and energy savings.

Table 3: Comparison to other implementations in literature, where all technology processes were scaled to 65 nm and number of receivers scaled to a single receiver chain.

Design	8-Bit*	Sign-Bit*	[6]	[27]	[7]
Technology [nm]	65	65	180	250	180
Quant. bits	8	1	10	10	10
Gate count	30K	8K	37K	-	104K
Vdd Core [V]	1.2	1.2	-	2.5	-
Area [mm^2]	0.06	0.02	-	0.42	0.196
Power [mW]	1.4	0.2	14	13.5	26.5

Scaling rules: A$\sim 1/s^2$ and P$\sim$(1/s)(Vdd/Vdd'). Vdd for 180 nm assumed to be 1.6 V.
*Down-scaled architecture to support only WLAN for fair comparison. In addition capable of estimating SNR.

7 Conclusions

This paper has demonstrated that it is possible to estimate symbol timing, CFO, and SNR only with the use of the received SB. It has also shown its advantages and disadvantages in terms of hardware complexity and performance as well as that these estimation techniques cover several OFDM standards by the realization of a multi-standard architecture. Performance simulations under realistic LTE scenarios indicate little or no degradation for symbol-timing and CFO estimation in comparison to higher resolution equivalent, whereas for SNR estimation the performance of SB is similar to its higher precision equivalent with much lower complexity. The potential of SB estimation techniques for low power receiver terminals was demonstrated with post-layout power simulations with back-annotated information. To this effect, it was shown that SB-estimation architecture dissipated at least 1/70 of the power consumption compared to similar existing works in the open technical literature. Finally, measurements of the time-frequency correlator have been presented and showed an average power consumption 0.62 mW for LTE with 20 MHz bandwidth and power supply of 1.2 V.

References

1. 3GPP: R4-070572 proposal for LTE channel models. Tech. rep., 3rd Generation Partnership Project Std (2007)
2. 3GPP: TS 36.213 v8.3.0 physical layer procedures. Tech. rep., 3rd Generation Partnership Project (2008)
3. Attallah, S., Wu, Y., Bergmans, J.: Low complexity blind estimation of residual carrier offset in orthogonal frequency division multiplexing based. IET Communications **1**(4), 604–611 (2007)
4. Beaulieu, N.: A useful integral for wireless communication theory and its application to rectangular signaling constellation error rates. IEEE Trans. Commun. **54**(5) (2006)
5. van de Beek, J., Sandell, M., Börjesson, P.: ML estimation of time and frequency offset in OFDM systems. IEEE Trans. Signal Process. **45**(7), 1800–1805 (1997)
6. Cho, J., Cho, Y., Islam, M., Kim, J., Cho, W.K.: Hardware-efficient auto-correlation for synchronization of MIMO-OFDM WLAN systems. In: International SoC Design Conference (ISOCC), pp. 560–563 (2009)
7. Cho, J., Kim, J., Cho, W.: VLSI implementation of auto-correlation architecture for synchronization of MIMO-OFDM WLAN systems. Journal of Semiconductor Technology and Science **10**(3) (2010)

8. Classen, F., Meyr, H.: Frequency synchronization algorithms for OFDM systems suitable for communication over frequency selective fading channels. In: IEEE 44th Vehicular Technology Conference (VTC), vol. 3, pp. 1655–1659 (1994)
9. Constantinides, G., Woeginger, G.: The complexity of multiple wordlength assignment. Applied Mathematics Letters **15**(2), 137 – 140 (2002)
10. Constantinides, G.A., Cheung, P.Y.K., Luk, W.: Multiple precision for resource minimization. In: IEEE Symposium on Field-Programmable Custom Computing Machines, FCCM '00, pp. 307–308. IEEE Computer Society, Washington, DC, USA (2000)
11. Cooper, K.D., Simpson, L.T., Vick, C.A.: Operator strength reduction. ACM Transactions on Programming Languages and Systems (TOPLAS) **23**(5), 603–625 (2001)
12. Dahlman, E., Parkvall, S., Skold, J.: 4G: LTE/LTE-Advanced for Mobile Broadband. Academic Press (2011)
13. Diaz, I., Wilhelmsson, L., Rodrigues, J., Löfgren, J., Olsson, T., Öwall, V.: A sign-bit auto-correlation architecture for fractional frequency offset estimation in OFDM. In: Proceedings of 2010 IEEE International Symposium on Circuits and Systems (ISCAS) (2010)
14. Fan, W., Choy, C.S.: Robust, low-complexity, and energy efficient downlink baseband receiver design for MB-OFDM UWB system. IEEE Trans. Circuits and Syst. I, Reg. Papers **59**(2), 399–408 (2012)
15. Horlin, F., Bourdoux, A.: Digital compensation for analog front-ends: a new approach to wireless transceiver design. Wiley (2008)
16. Keller, T., Hanzo, L.: Orthogonal frequency division multiplex synchronisation techniques for wireless local area networks. In: Seventh IEEE International Symposium on Personal Indoor and Mobile Radio Communications (PIMRC), vol. 3, pp. 963–967 (1996)
17. Lmai, S., Bourre, A., Laot, C., Houcke, S.: An efficient blind estimation of carrier frequency offset in OFDM systems. IEEE Trans. Veh. Technol. (99), 1–1 (2013)
18. Meher, P., Valls, J., Juang, T.B., Sridharan, K., Maharatna, K.: 50 years of CORDIC: Algorithms, architectures, and applications. IEEE Trans. Circuits and Syst. I, Reg. Papers **56**(9), 1893–1907 (2009)
19. Moose, P.H.: A technique for orthogonal frequency division multiplexing frequency offset correction. IEEE Trans. Commun. **42**(10), 2908–2914 (1994)
20. Pham, T.H., McLoughlin, I.V., Fahmy, S.A.: Robust and efficient OFDM synchronization for FPGA-based radios. Circuits, Systems, and Signal Processing pp. 1–19 (2014)
21. Prudnikov, A., Brychkov, Y., Marichev, O.: Integrals and series. Gordon and Breach Science Publishers (1992)
22. Schmidl, T., Cox, D.: Robust frequency and timing synchronization for OFDM. IEEE Trans. Commun. **45**(12), 1613–1621 (1997)
23. Sesia, S., Toufik, I., Baker, M.: LTE - The UMTS Long Term Evolution: From Theory to Practice. John Wiley and Sons (2009)
24. Speth, M., Fechtel, S., Fock, G., Meyr, H.: Optimum receiver design for OFDM-based broadband transmission part II. A case study. IEEE Trans. Commun. **49**(4), 571–578 (2001)
25. Stott, J.H.: The effects of frequency errors in OFDM. Tech. rep., BBC RD (1995)
26. Sun, M.F., Yu, J.Y., Hsu, T.Y.: Estimation of carrier frequency offset with I/Q mismatch using pseudo-offset injection in OFDM systems. IEEE Trans. Circuits and Syst. I, Reg. Papers **55**(3), 943–952 (2008)
27. Troya, A., Maharatna, K., Krstic, M., Grass, E., Jagdhold, U., Kraemer, R.: Low-power VLSI implementation of the inner receiver for OFDM-based WLAN systems. IEEE Trans. Circuits Syst. I, Reg. Papers **55**(2), 672–686 (2008)
28. Tufvesson, F., Edfors, O., Faulkner, M.: Time and frequency synchronization for OFDM using PN-sequence preambles. In: IEEE VTS 50th Vehicular Technology Conference - Fall (VTC), vol. 4, pp. 2203–2207 (1999)
29. Vachhani, L., Sridharan, K., Meher, P.: Efficient CORDIC algorithms and architectures for low area and high throughput implementation. IEEE Trans. Circuits and Syst. II, Exp. Briefs **56**(1), 61–65 (2009)
30. Whalen, A.D.: Detection of signals in noise. New York : Academic Press (1971)
31. Wilhelmsson, L., Diaz, I., Olsson, T., Öwall, V.: Performance analysis of sign-based pre-FFT synchronization in OFDM systems. In: IEEE 71st Vehicular Technology Conference - Spring (VTC), pp. 1–5 (2010)
32. Wilhelmsson, L., Diaz, I., Olsson, T., Öwall, V.: Analysis of a novel low complex SNR estimation technique for OFDM systems. In: IEEE Wireless Communications and Networking Conference (WCNC), pp. 1646–1651 (2011)
33. Zhang, J., Zhang, Z., Zhou, S., Tan, M., Liu, X., Cheng, X., Cong, J.: Bit-level optimization for high-level synthesis and FPGA-based acceleration. In: Proceedings of the 18th annual ACM/SIGDA International Symposium on Field Programmable Gate Arrays, pp. 59–68 (2010)
34. Zhang, L., Zhang, Y., Zhou, W.: Floating-point to fixed-point transformation using extreme value theory. In: Eighth IEEE/ACIS International Conference on Computer and Information Science (ICIS), pp. 271–276 (2009)